PROBLEMS ASSOCIATED WITH THE ELASTICITY OF LIQUIDS

D. D. Joseph

Department of Aerospace Engineering and Mechanics
University of Minnesota, Minneapolis, MN 55455

These lectures are in three parts:

1. Physical phenomena associated with hyperbolicity and change of type;

2. Conceptual ideas associated with effective viscosities and rigidities and the origins of viscosity in elasticity;

3. Mathematical problems associated with hyperbolicity and change of type.

The ideas which I will express in these lecture are very condensed forms of ideas which have been put forward in various papers and most completely in my recent book *Fluid Dynamics of Viscoelastic Liquids,* published in 1990 by Springer-Verlag. The mathematical theory of hyperbolicity and change of type is associated with models with an instantaneous elastic response. Basically, this means that there is no Newtonian like part of the constitutive equation. The theory for these models as it is presently known is in my book. I am persuaded that further development of this subject lies in the realm of physics rather than mathematics. The main issues are centered around the idea of the effective viscosity and rigidity and the measurements of slow speeds, topics which are discussed in this paper in a rather more discursive than mathematical manner.

1. PHYSICAL PHENOMENA ASSOCIATED WITH HYPERBOLICITY AND CHANGE OF TYPE

It is well known that small amounts of polymer in a Newtonian liquid can have big effects on the dynamics of flow. Drag reductions of the order of 80% can be achieved by adding polymers in concentrations of fifty parts per million to water. This minute addition does not change the viscosity of the liquid but evidently has a strong effect on other properties of the liquid which have as yet been inadequately identified.

We are going to consider some effects of adding minute quantities of polyethylene oxide to water on the flow over wires. The first experiments were on uniform flow with velocity U across small wires, flow over a cylinder. James and Acosta [1970] measured the heat transferred from three wires of diameter D=0.001, 0.002 and 0.006 inches. They used three different molecular weights of polymers in water (WSR 301, 205 and coagulant) in concentrations ϕ ranging from 7 parts to 400 parts per million by weight, the range of extreme dilution, in the drag reduction range. They found a critical velocity U_c in all cases except the case of most extreme dilution ϕ=6.62 ppm, as is shown in Figure 1. A brief summary of the results apparent in this figure follows.

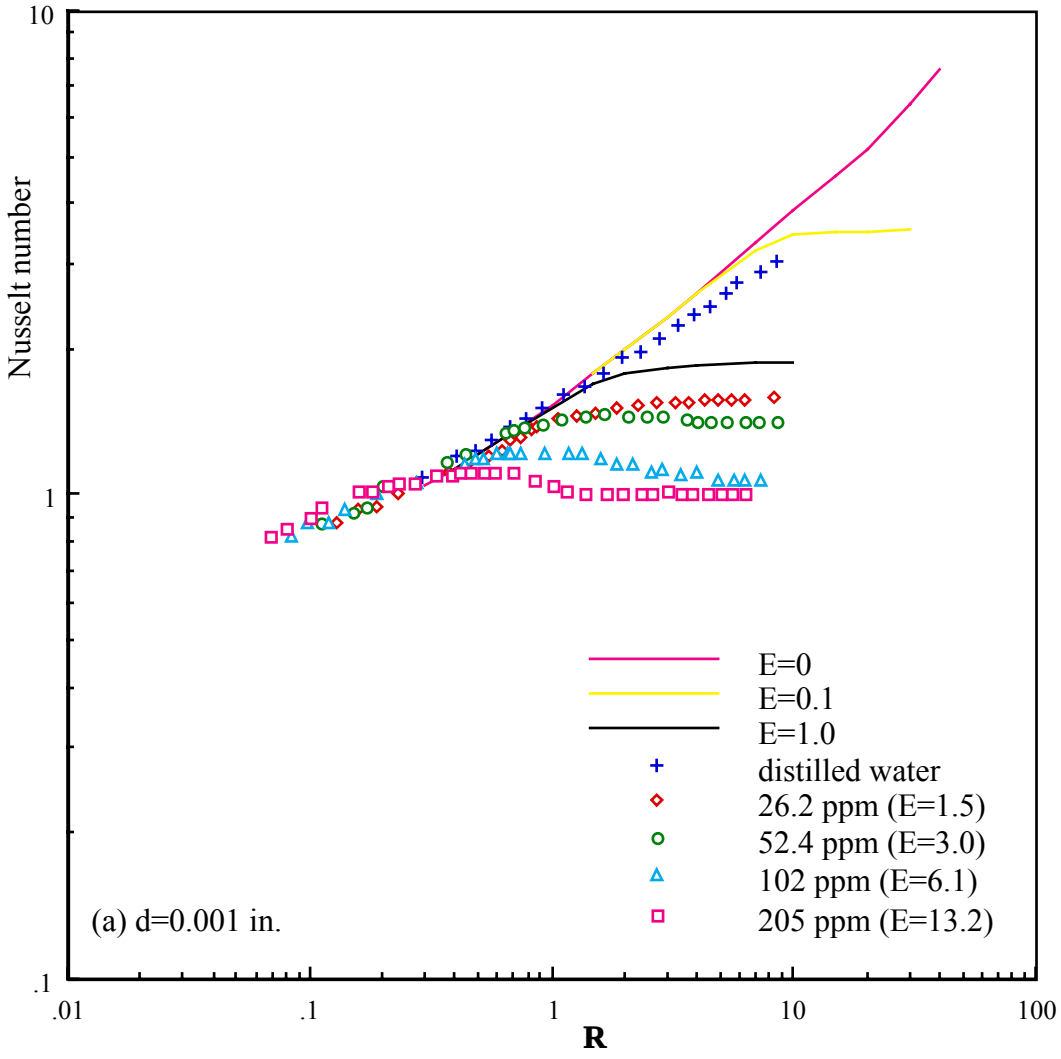
10
1
.1
Nusselt number
.01
.1
1
10
100
R
E=0
E=0.1
E=1.0
distilled water
26.2 ppm (E=1.5)
52.4 ppm (E=3.0)
102 ppm (E=6.1)
205 ppm (E=13.2)
(a) d=0.001 in.

(a)

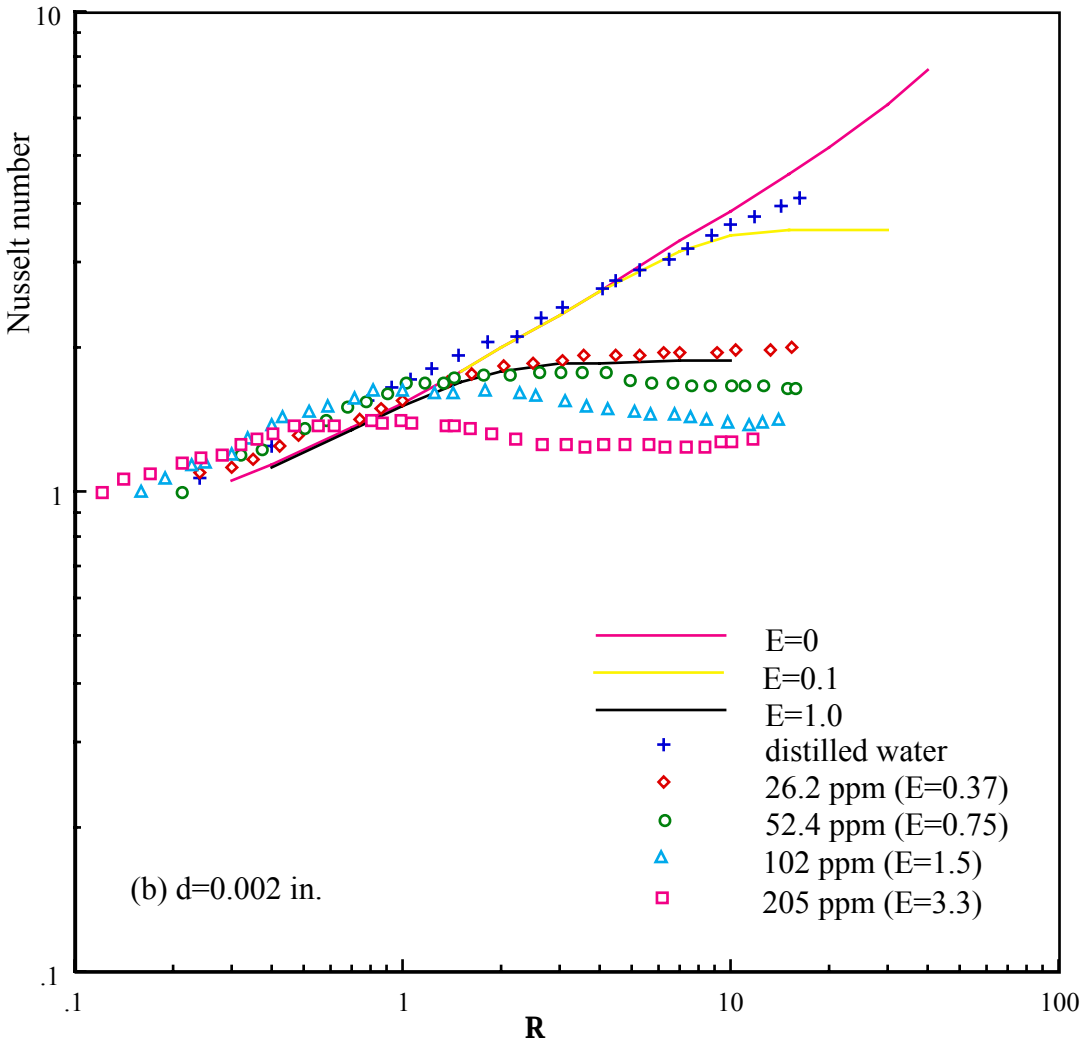
10
1
.1
.1
1
10
100
Nusselt number
R
(b) d=0.002 in.
E=0
E=0.1
E=1.0
distilled water
26.2 ppm (E=0.37)
52.4 ppm (E=0.75)
102 ppm (E=1.5)
205 ppm (E=3.3)

(b)

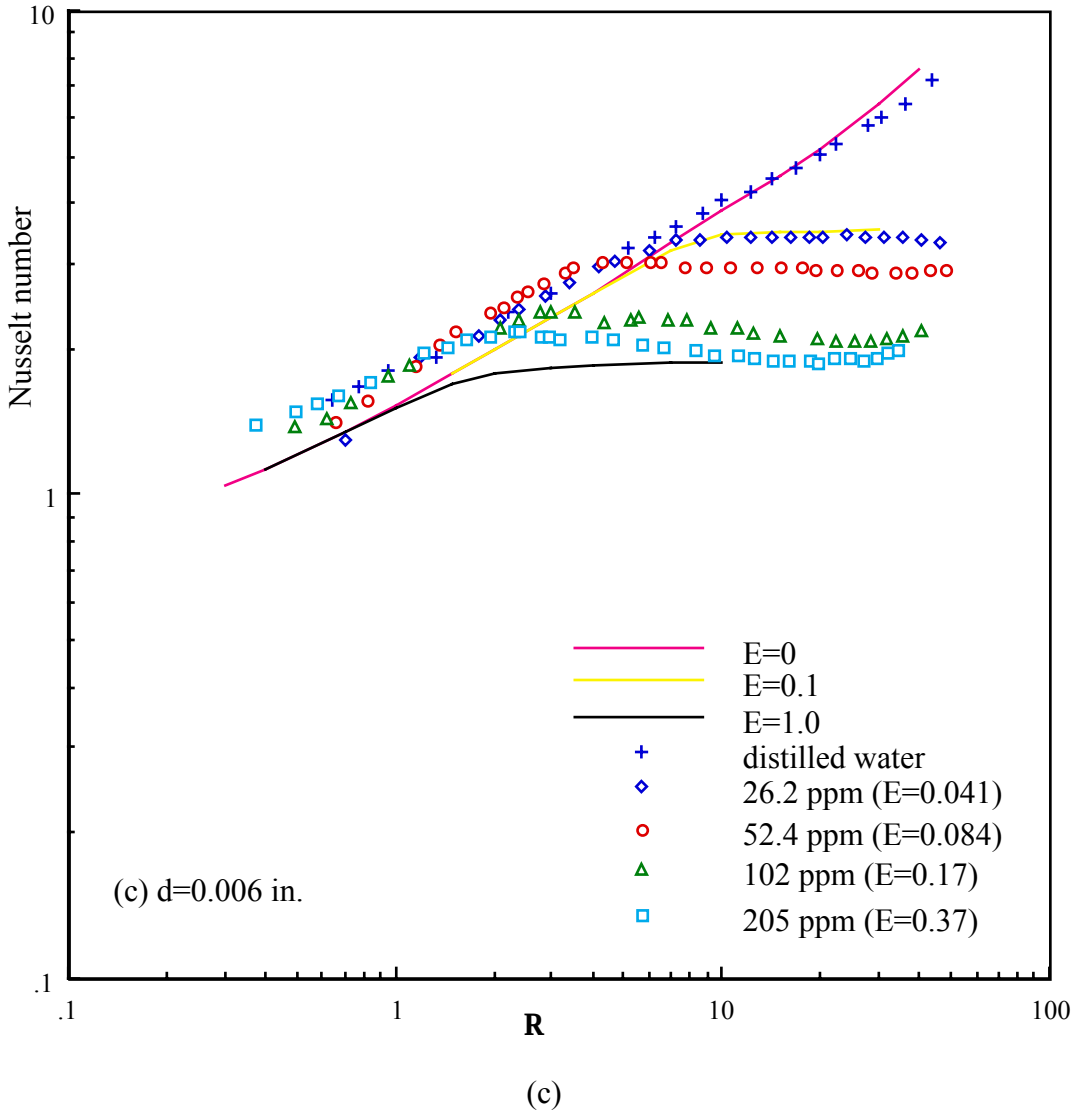

(c)

Figure 1 Heat transfer from heated wires of WSR 301 (after James and Acosta [1987]). The experimental points are dots and the lines are from computations of Hu and Joseph [1990]. (a) d=0.001 in. (b) d=0.002 in. (c) d=0.006 in.

1. There is a critical value U_c for all but the most dilute solutions: When $U<U_c$, the Nusselt number Nu(U) increases with U as in a Newtonian fluid. For $U>U_c$, the Nusselt number becomes independent of U as in Figure 1.

2. U_c is independent of the diameter of the wire. This is remarkable. It suggests that U_c is a material parameter depending on the fluid alone.

3. U_c is a decreasing function of ϕ, the concentration. It is useful to note once again that in the range of ϕ between 6 ppm to 400 ppm, the viscosity is essentially constant and equal to the viscosity of water.

Ambari, Deslouis, and Tribollet [1984] obtained results for the mass transfer from 50 micron wires in a uniform flow of aqueous polyox (coagulant) solution in concentrations of 50, 100, and 200 parts per million. Their results are essentially identical to those obtained by James and Acosta [1970]; there is a critical U_c, a decreasing function of ϕ, signalling a qualitative change for the dependence of the mass transport of U, from a Newtonian dependence when $U<U_c$, to a U independent value for $U>U_c$. Their values of U_c for the break in the mass transport curve are just about the same as the value of U_c found by James and Acosta for heat transfer.

Ultman and Denn [1970] suggested that $U_c=c=\sqrt{\eta/\lambda\rho}$ where η is the viscosity, λ the relaxation time, and ρ is the density of a fluid whose extra stress $\boldsymbol{\tau}=\mathbf{T}+p\mathbf{1}$ satisfies Maxwell's equation

$$\lambda U\partial\boldsymbol{\tau}/\partial x+\boldsymbol{\tau}=\mu[\ \mathbf{u}=\ \mathbf{u}^T] \tag{1}$$

where $\mathbf{u}$ is the velocity. They used the molecular theory of Bueche to find the value of the relaxation time λ_B for the 52.4 ppm solution and they found that a $0.7\lambda_B$ would give $\sqrt{\eta/0.7\lambda_B}$ $=U_c\sim 2.9$ cm/sec., that is, their estimate of λ_B from Bueche's theory is almost good enough to give $c=U_c$. Their calculation of the time of relaxation cannot be relevant, however, because in the Bueche theory

$$\lambda_B=\frac{12M\eta_s(10^3+12\phi)}{10^6\pi^2RgT} \tag{2}$$

does not go to zero with the concentration ϕ. The quantities in (2) are (M, η_s, Rg, T)=(molecular weight, the viscosity of water, the gas constant, absolute temperature). The zero ϕ value of λ_B can be interpreted as a relaxation time for a single polymer in a sea of solvent. The relaxation

time of one polymer cannot be the relaxation time of the solution in the limit in which the polymer concentration tends to zero, because in this limit the solution is all solvent.

Joseph, Riccius and Arney [1986] measured c=2.48 cm/sec in a 50 ppm, WSR 301 aqueous solution. This measurement supports the idea that U_c=c. We are trying now to measure wave speeds in extremely dilute solutions in the drag reduction range. We find considerable scatter in our data in these low viscosity solutions and are at present uncertain about the true value of the effective wave speed, including the values which we reported earlier.

The hypothesis that U_c=c is consistent with the following argument about the dependence of the wave speed on concentration. In the regime of extreme dilution, the viscosity does not change with concentration. However, there appears to be a marked effect on the average time of relaxation which increases with concentration. It follows then that the wave speed $c=\sqrt{\eta/\rho\lambda}$ must decrease with concentration ϕ.

The shear viscosity for dilute polymers can be calculated using

$$\eta = \eta_s(1 + [\eta]\phi) \tag{3}$$

where $[\eta]=(\eta-\eta_s)/\phi$ is the intrinsic viscosity. It has a definite value as $\phi\varnothing 0$. James and Acosta [1970] and James and Gupta [1971] developed expressions of the form $\lambda=A\phi$ from molecular theory. A is a function of the polymer properties and it can even be a slowly varying function of ϕ. They find that

$$A = \frac{2}{5}\,\frac{\eta_s[\eta]^2 M}{RgT} \quad . \tag{4}$$

This expression shows that λ is proportional both to the largest relaxation time of polymer molecules $\lambda_m=\eta_s[\eta]n/\pi^2 RgT$ and to the concentration ϕ. James and Gupta [1971] generalized the derivation and showed significant influence of molecular weight distribution on the magnitude of the relaxation. They found that $\lambda=A\phi$, with A given by (4) could possibly

underestimate the value of the relaxation time computed as a mean value from a two relaxation time model by a factor of order 10, depending on the molecular weight distribution of the polymers.

If at small concentrations ϕ, $\lambda=A\phi$ with A independent of ϕ, then the wave speeds $c=\sqrt{\eta/\lambda\rho}$ of dilute polymer solutions of two concentrations ϕ_1 and ϕ_2 are given by

$$c_2 = c_1 \sqrt{\frac{\phi_1}{\phi_2}} \sqrt{\frac{1+[\eta]\phi_2}{1+[\eta]\phi_1}} \quad .$$

for extremely dilute solutions $[\eta]\phi \ll 1$ and we find that

$$c = \sqrt{\eta_s/\rho A\phi} \quad = C\phi^{1/2} \tag{5}$$

where $\lambda=A\phi$ and η_s, A, ρ and C are independent of ϕ.

In Figure 2 we have plotted the critical velocity versus concentration for three polyox solutions and the three diameters of wires used in the experiments. We see that the line $U_c=C\phi^{1/2}$ fit the data of James and Acosta quite well. This lends support to the notion that the critical speed is equal to the shear wave speed $U_c=c$ in some approximate sense. We note that the attempt of Ultmann and Denn [1971] to fit the concentration data (their Figure 3) failed because they used the Bueche relaxation time (2) rather than the linear relation $\lambda=A\phi$, with A determined from a measurement using the wave speed meter.

We shall return to compare these observations with direct numerical simulations in part 3 of this paper.

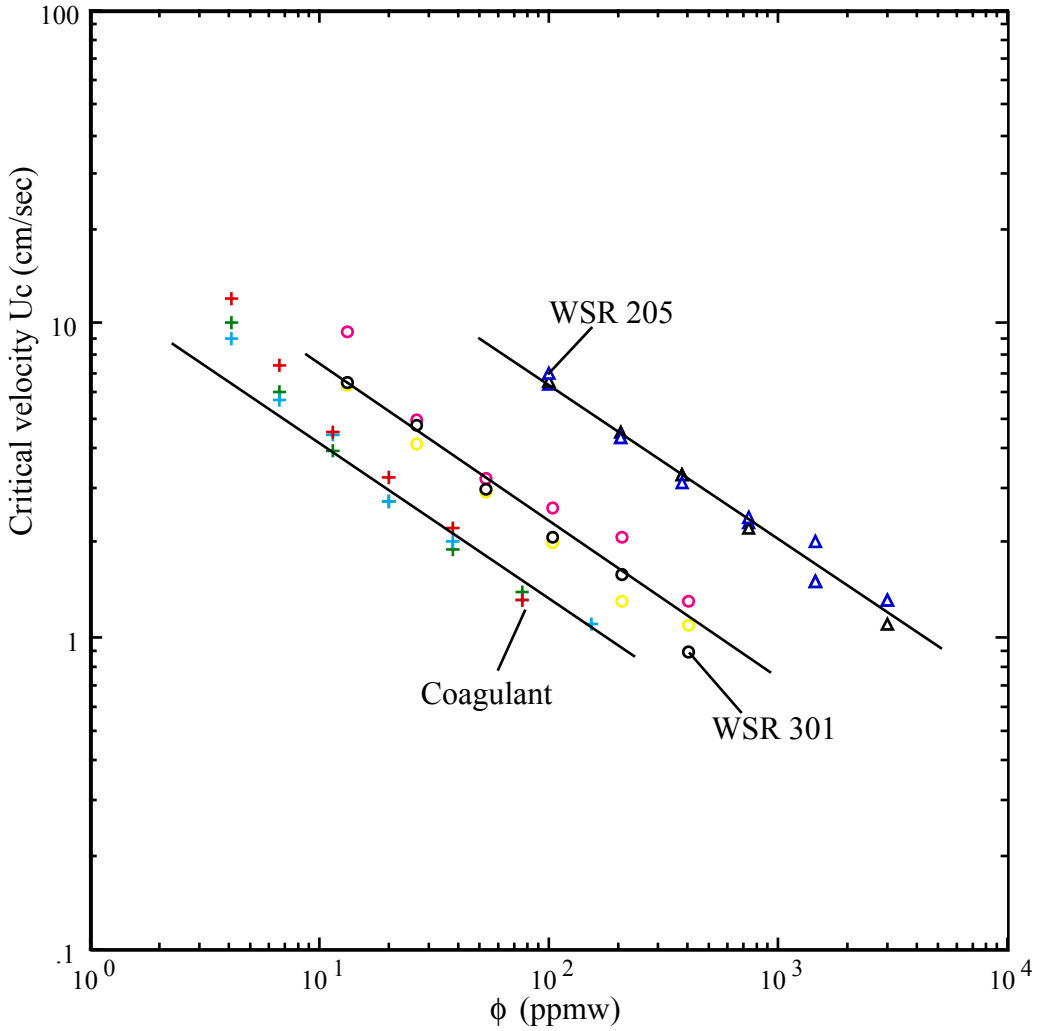

Figure 2 Critical velocity at which the Nusselt number starts to deviate from the Newtonian data versus concentration for three Polyox solutions (WSR-205, WSR-301, coagulant) and three cylindrical wires (d=0.001, 0.002, 0.006in.). Data of James and Acosta [6]. Solid lines are correlations $U_c = C\ \phi^{-1/2}$.

Konuita, Adler and Piau [1980] studied the flow around a 0.206 mm wire in an aqueous polyox solution (500 ppm, WSR-301) using laser-Doppler techniques. They found a kind of shock wave in front of the cylinder, like a bow shock. They say that the velocity of the fluid is zero in a region fluid in front of the stagnation point. Basically they say that there is no flow, or very slow flow near the cylinder. The formation of the shock occurs at a certain finite speed, perhaps U_c. This type of shock is consistent with the other observations in the sense that with a stagnant region around the cylinder, the transport of heat and mass could take place only by

diffusion, without convection. This explains why there is no dependence of the heat and mass transfer on the velocity when it exceeds a critical value.

I estimated the critical speed, using the data of Konuita, Adler and Piau, and I estimated the wave speed c by extrapolating from our measurements in the polyox solutions at different concentrations. These estimates are reported in my book "Fluid Dynamics of Viscoelastic Liquids." They are consistent with the notion of a supercritical shock transition at U_c=c.

Another striking phenomenon which appears to be associated with a supercritical transition is delayed die swell. It is well known that polymeric liquid will swell when extruded from small diameter pipes. The swelling can be very large, four, even five times the diameter of the jet. This swelling is still not well understood even when there is no delay. Joseph, Matta and Chen [1987] have carried out experiments on 19 different polymer solutions. They found that there is a critical value of the extrusion velocity U_c such that when $U<U_c$, the swell occurs at the exit, but when $U>U_c$ the swell is delayed, as in Figure 3. If U is taken as the centerline velocity in the pipe, then the transition is always supercritical with U_c>c. The length of the delay increases with U. The velocity in the jet after the swell of jet has fully swelled is subcritical $U_f<U$ where U_f is the final U. This is something like a hydraulic jump with supercritical flow ahead of the delay and subcritical flow behind it.

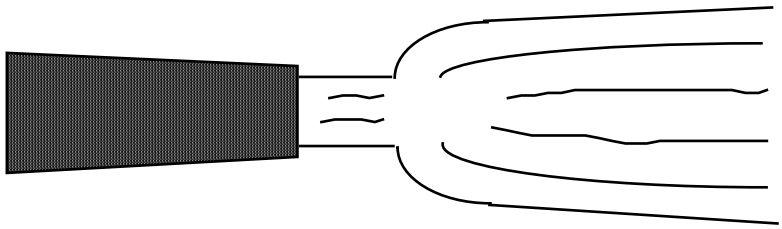

Figure 3 Delayed die swell.

Yoo and Joseph [1985] studied Poiseuille flow of an upper convected Maxwell model through a plane channel. Ahrens, Yoo and Joseph [1987] studied the same problem in a round pipe. In both cases, we get a hyperbolic region of flow in the center of the pipe when the

centerline velocity U_m, equal to 2U in the Maxwell model, is greater than the wave speed c. This gives theoretical support to the idea that delayed die swell is a supercritical phenomenon.

There is a marked difference between the shape of the swell when it is delayed between different polymer solutions. The shape seems to correlate with a relaxation time

$$\lambda = \tilde{\mu} / G_c \tag{2}$$

where $\tilde{\mu}$ is the zero shear rate viscosity and G_c is the rigidity. We get G_c from measuring c

$$c^2 = G_c/\rho \, . \tag{3}$$

When λ is large, say $\lambda \geq 0(10^{-3}$ sec), the delay is sharp, as in Figure 3. When the relaxation times are small, $\lambda \leq 0(10^{-4}$ sec), the delay is smoothed; in the extreme cases it is difficult to see that the swell is actually delayed.

We can say the Newtonian fluids are fluids with very large values of λ. In the case of delayed die swell, the smoothing of the swell is probably associated by the effect of smoothing due to an effective viscosity which arises from rapidly relaxing modes which have already relaxed when the delayed swell commences. Very viscous liquids always exhibit relaxation or non-Newtonian effects because even though the relaxation is fast, there is so much to relax.

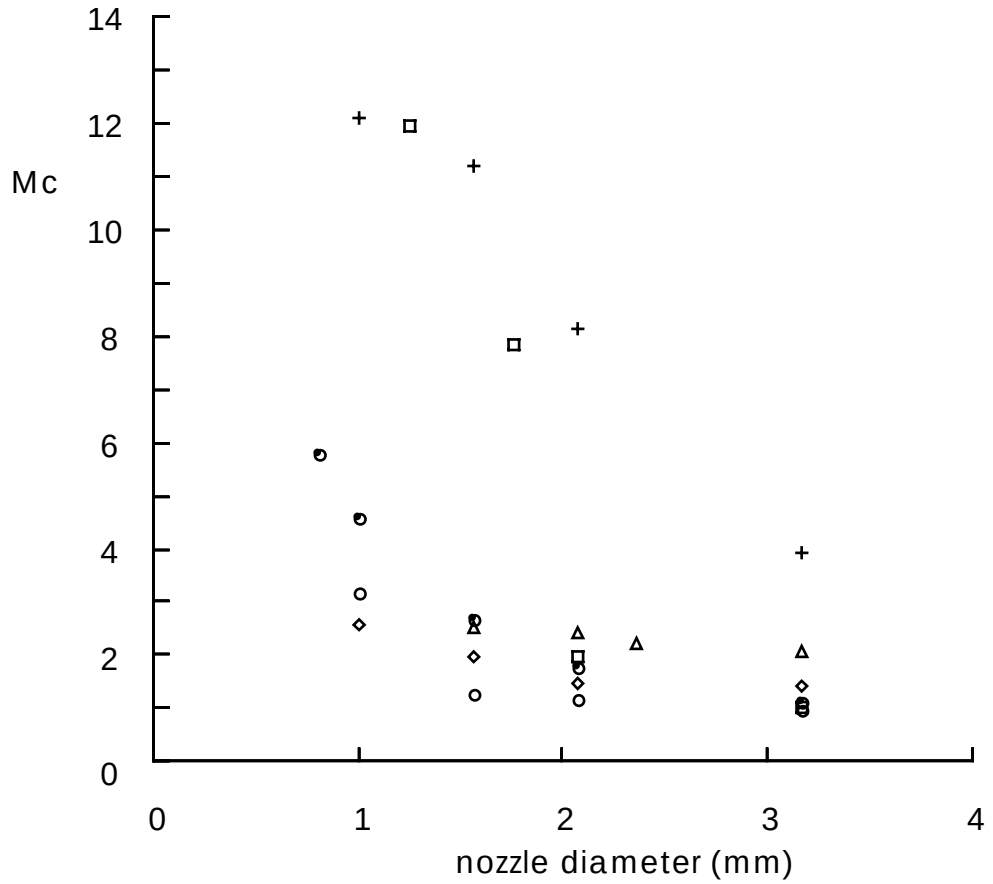

Figure 4 Mach number vs. pipe diameter.

○ **1.3% CMC** □ **9.8% ELVACITE** ◇ **6% PIB/D**

◕ **2.5% POLYOX** + **12.1% K-125** △ **M-1**

In Figure 4, we plotted the critical Mach number

$M_c = 2U_c/c$

against the diameter of the pipe. In all cases $M_c \geq 1$, nearly. The value $M_c=1$ seems to be some form of asymptote for large values of the pipe diameter d. We do not understand why different fluids have such different M_c vs. d curves. We have thought about the consequences of shear thinning, which are important for some of the test liquids, in trying to collapse the experimental curves for different liquids into one curve, but we have not been successful.

Delvaux and Crochet [1989] have done a numerical study of delayed die swell in a plane jet using an Oldroyd B model, the upper convected Maxwell model plus a very small perturbing Newtonian viscosity μ such that $\mu/(\mu+\eta)=0.05$. The results of their calculation are very interesting. They confirm the conjectures of Joseph, Matta and Chen [1987] which have been expounded, and introduce some new understandings. The main new result can be described as "the breakout of the region of the hyperbolic vorticity." At small supercritical values of the velocity (Mach numbers not too greatly in excess of one) the hyperbolic region extends slightly downstream into the jet but does not touch the jet boundary, as can be seen in panel (a) and (b) of Figure 5.

As the velocity increases, more and more of the jet is consumed by the hyperbolic region. At a certain velocity, between panel (b) and (c) of Figure 5, the hyperbolic region first touches the jet boundary, then consumes more and more of the jet boundary. Evidently the change in the curvature of the jet is associated with the breakout of the hyperbolic region. This explains why the delay is not observed at small supercritical values of the velocity but only at larger postcritical breakout values. It would be good if we could find a way to explain the way the delay depends on the jet diameter.

Figure 5 (after Delvaux and Crochet, 1989). Jet profile and hyperbolic regions of vorticity under different conditions in a plane jet of an Oldroyd B fluid with a very small Newtonian viscosity. (a) (M, R,W)=(2.3, 13.5, 0.39); (b) (2.9, 17, 0.49); (c) (4.1, 29.9, 0.87), (d) (5.1, 34.6, 1)

2. CONCEPTUAL IDEAS

Nonlinear constitutive modeling is a jungle. The possible responses of the material to stresses are too complicated to describe by one explicit expression. General expressions are too abstract to be of direct use and are always insufficiently general to describe everything. Linearizing around rest is good because many different models collapse to one. The nonlinear

parameters go away. Moreover, the elasticity of liquids is preeminently associated with propagation of small amplitude waves into rest.

We start with Boltzmann's expression for the extra stress $\boldsymbol{\tau}$ which has been generalized to contain a Newtonian term

$$\boldsymbol{\tau} = 2\mu\mathbf{D}\,[u(\mathbf{x}, t)] + 2\int_0^\infty G(s)\mathbf{D}[\mathbf{u}(\mathbf{x}, t-s)]ds \tag{6}$$

where $\mathbf{u}$ is the velocity, $\mathbf{D}$ is the symmetric part of grad $\mathbf{u}$ and G(s) is positive, bounded and monotonically decreasing to zero. The actual stress $\mathbf{T}=-p\mathbf{1}+\boldsymbol{\tau}$ differs from $\boldsymbol{\tau}$ by a "pressure" p. Equation (6) is the most general linear functional of grad $\mathbf{u}$ in a fluid. To name a fluid, we need a Newtonian viscosity μ and a shear relaxation modulus G(s). We get Jeffreys' model from (6) when we write $G(s)=\frac{\eta}{\lambda}\exp(-s/\lambda)$ and Jeffreys' model reduces to Maxwell's if also $\mu=0$.

Now we consider viscosity. In steady flow, $\mathbf{u}$ is independent of t and comes out of the integral in (6). We get

$$\boldsymbol{\tau} = 2\tilde{\mu}\,\mathbf{D}[\mathbf{u}(\mathbf{x})]$$

where $\tilde{\mu}=\mu+\eta$ is the static or zero shear viscosity and $\eta=\int_0^\infty G(s)ds$, the area under G(s), is the elastic viscosity. We have a viscosity inequality $\tilde{\mu}\geq\eta$ with equality when there is no Newtonian viscosity $\mu=0$.

Now we consider elasticity $\mu=0$, writing

$$\mathbf{D}[\mathbf{u}(\mathbf{x}, t-s)] = -\frac{\partial}{\partial s}\,\mathbf{E}\,[\boldsymbol{\xi}(\mathbf{x}, t-s)]$$

where $\boldsymbol{\xi}$ is a displacement and **E** is the infinitesimal strain. If it were possible to make a step in strain without flow, and it isn't possible, we would have $\mathbf{D}[\mathbf{u}(\mathbf{x}, t)] = \mathbf{E}_0(x)\delta(t)$ for Dirac δ. Then, from (6), with $\mu=0$,

$$\boldsymbol{\tau} = 2G(t)\, \mathbf{E}_0(\mathbf{x})$$

and you can see why G(t) is called the stress relaxation function and G(0) the rigidity or shear modulus. Another way to see elasticity with $\mu=0$ is to write

$$\boldsymbol{\tau} = 2\int_0^\infty -\frac{\partial}{\partial s}\, \{G(s)\mathbf{E}\,[\boldsymbol{\xi}\,(\mathbf{x}, t-s)]\}ds + 2\int_0^\infty G'(s)\mathbf{E}\,[\boldsymbol{\xi}\,(\mathbf{x}, t-s)]\, ds\,. \tag{7}$$

Now we can suppose that G(s) decays ever so slowly so that the second integral will tend to zero while the first gives rise to linear elasticity for an incompressible solid

$$\boldsymbol{\tau} = 2G(0)\, \mathbf{E}\,[(\boldsymbol{\xi}\,(\mathbf{x}, t)]. \tag{8}$$

Now we restore the Newtonian viscosity and we note that this viscosity smooths discontinuities. For example, in the problem of the suddenly accelerated plate, the boundary at y=0 below a semi-infinite plate is suddenly put into motion, sliding parallel to itself with a uniform speed. If $\mu=0$, this problem is governed by a telegraph equation. The news of the change in the boundary value from zero to constant velocity propagates into the interior by a damped wave with a velocity $c=\sqrt{G(0)/\rho}$. The amplitude of the velocity shock decays exponentially. A short while after the wave passes, the solution at the given y looks diffusive. If $\mu\neq0$, and is small, a sharp front cannot propagate. Instead we get a shock layer whose thickness is proportional to $\sqrt{\mu y/\tilde{\mu}}$ and the solution, as in the Newtonian fluid, is felt instantly everywhere. We get a diffusive signal plus a wave. The wave could be dominant in the dynamics if μ is small.

Actually diffusion is impossible because it requires that a pulse initiated at any point be felt instantly everywhere. This same defect hold for all models with $\mu \neq 0$, like Jeffreys'. Propagation should proceed as waves.

Poisson, Maxwell, Poynting and others thought that $\mu=0$ ultimately. It's all a matter of time scales. Short range forces between molecules of a liquid give rise to weak clusters of molecules which resist fast deformations elastically, then relax. Liquids are closer to solids than to gases. Liquid molecules do not bounce around with a mean free path, they move cooperatively.

So what is the difference between two liquids with the same η, one appearing viscous (Newtonian) and the other elastic? Maxwell thought that viscous liquids were actually elastic, with high rigidity and a single fast time of relaxation. To fix his idea in your mind, we compare two liquids with the same viscosity η, satisfying Maxwell's model with $G(s)=G(0)\exp(-s/\lambda)$, $G(0)=\eta/\lambda$. To have the same η the Newtonian liquid would have a relatively large $G(0)$ and a small time λ of relaxation. The trouble with Maxwell's model, if not his idea, is that a single time of relaxation is against experiments which can never be made to fit a single time of relaxation.

There are many different times of relaxation. Experiments indicate that many liquids respond to high frequency ultrasound like a solid organic glass with

$$G(0) \sim 10^9 \text{Pa}, \; c=\sqrt{G(0)/\rho} \sim 10^5 \text{ cm/sec.} \tag{9}$$

This type of estimation is valid for a huge range of liquids, from olive oil to high molecular weight silicon oils. With this time of relaxation and such a high rigidity, all the liquids would look Newtonian, with t much greater than $\tilde{\mu}/G(0)$, which is of the order of 10^{-10} sec. in olive oil, and is perhaps 10^{-6} in some high viscosity silicon oils. In fact, we see much longer lasting responses which come about because there are different times of relaxation. Small molecules

relax rapidly, giving rise to large rigidity G(0) and fast speed. Large molecules and polymers relax slowly, giving rise to a smaller effective rigidity $G_\mu(0)$, effective viscosity μ and slow speed

$$c=c_\mu=\sqrt{G_\mu(0)/\rho}\ . \tag{10}$$

To get this firmly in mind, we can think of a kernel with values like those given by (9), sketched in Figure 6.

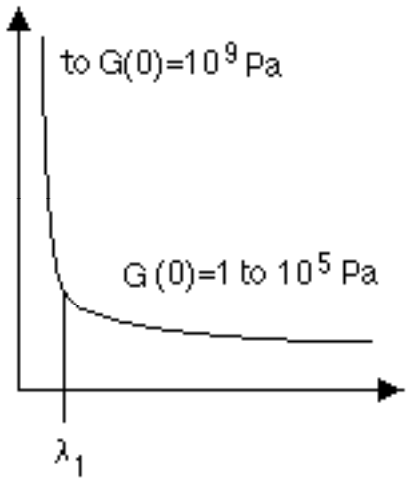

Figure 6 G(s), fast relaxation (say 10^{-10} sec) followed by a slow relaxation (say 10^{-4} sec).

We may inquire if at $t>>10^{-10}$ sec the relaxed fast modes have a dynamical effect. Yes, they give rise to an effective viscosity. We may as well collapse the glassy mode into a one-sided delta function $\mu\delta(s)$ where $\mu=G(0)\lambda_1$, or some fraction of this. This is our effective viscosity and our construction shows that is not unique. This is a very interesting concept, but it is not amenable to experiments that we know.

It is useful to define a time unit in terms of the slowest relaxation, say $\tilde{\mu}/G_c$. This gives rise to an internal clock, with a material time defined by the slowest relaxation. This time may be slow or fast on the external clock. To get this idea, think of the analog for the transport of heat. Heat is transported in solids by fast waves. The fastest wave is associated with electrons with relaxation times of 10^{-13} sec, then by lattice waves (phonons) with relaxation times of 10^{-}

^{11} sec. Both times are surpassingly short on our clock. However, at 10^{-13} sec, the electrons have all relaxed (and they give rise to diffusion) whilst the phonons have not begun to relax. Of course, it's more interesting when the slow relaxation is not too fast on our clock, as is true for viscoelastic fluids.

The notion of an external and internal clock is an appealing idea for expressing the difference between different theories of fading memory. Some theories, like Maxwell's and the more mathematical one by Coleman and Noll [1960] use an external clock; in rapid deformations the fluid responds elastically; in slow deformations the response is viscous. Fast and slow are measured in our time, on the external clock. Such theories rule out transient Newtonian responses. Models with $\mu \neq 0$, like Jeffreys', or the more mathematical one by Saut and Joseph [1983], are disallowed. To get $\mu \neq 0$ back in, even though ultimately $\mu = 0$, we need an effective μ, associated with an internal clock.

3. MATHEMATICAL THEORY

When the fluid is elastic the governing equations are partly hyperbolic. The hyperbolic theory makes sense when the Newtonian viscosity is zero or small relative to the static viscosity $\tilde{\mu}$. For very fast deformations in which the fluid responds momentarily like a glass, the equations always exhibit properties of hyperbolic response, waves and change of type. However, the glassy response takes place in times too short to notice. Hence, the hyperbolic theory is not useful where it is exact. The hyperbolic theory is useful when we get an elastic response at times we read on our clock, in the domain of the effective theory. Hence, the hyperbolic theory is useful where it is not exact.

Most of the mathematical work has been done with fluids like Maxwell's and for plane flows. These problems are governed by six quasilinear equations in six unknowns. The unknowns are two velocity components, three components of the stress, and a pressure. The

continuity equation, two momentum equations and three equations for the stress govern the evolution of the six variables. The stress equations are like Maxwell's

$$\lambda\left[\frac{\partial \boldsymbol{\tau}}{\partial t}+\mathbf{u}\bullet\ \boldsymbol{\tau}+\boldsymbol{\tau}\boldsymbol{\Omega}-\boldsymbol{\Omega}\boldsymbol{\tau}-a(\mathbf{D}\boldsymbol{\tau}+\boldsymbol{\tau}\mathbf{D})\right] = 2\eta\mathbf{D} + \mathrm{l}$$

where $\mathbf{D}$ is the symmetric part and $\boldsymbol{\Omega}$ the antisymmetric part of $\mathbf{u}$, $-1\le a\le 1$ and l are lower order terms, algebraic in the system variables. This system may be analyzed for type in the usual way. We get a 6th order system and it factors into three quadratic roots. Two of the roots are imaginary so that the system is not hyperbolic. The streamlines are characteristic, with double roots so that the system is not strictly hyperbolic. The third quadratic factor depends on the unknown solution, algebraically, and it can be real or complex, depending on the solution. We say that such a solution with mixed roots is of composite type. Some variables are elliptic, some are hyperbolic.

It turns out that the pair of roots which depend on the unknown solution and can change type are associated with the vorticity equation, a second order nonlinear PDE. This equation is either elliptic or it is hyperbolic, depending on the solution. It is not of composite type, but is classical, like the equation for the potential in gas dynamics.

We can think of the unsteady vorticity equation and the steady vorticity equation. The analysis of the two has greatly different consequences. The unsteady equation is ill-posed when it is elliptic and well-posed when it is hyperbolic. Ill-posed problems are catastrophically unstable to short waves, with growth rates which go to infinity with the wave number. The conditions on the stress which lead to ill-posed problems can be determined by the method of frozen coefficients, as was first done by Rutkevich [1969]. It turns out that the Maxwell models with $a=\pm 1$ cannot be ill-posed on smooth solutions, but the other models do become ill-posed for certain flows.

The problem of change of type in steady flow is different. The vorticity in steady flow can be of mixed type with elliptic and hyperbolic regions, as in transonic flow. The physical implications of these mixed "transonic" fields are not yet perfectly understood, though many examples have been calculated.

There are many models, other than those like Maxwell's, in which vorticity is the key variable. It is the only variable which is either strictly elliptic or strictly hyperbolic. The stream function satisfies Laplace's equation, the velocity and the stresses are of composite type. The stresses do not satisfy a hyperbolic equation and it is wrong to speak of the propagation of stress waves.

There are other models in which the vorticity is not the key variable. However, when these models are linearized around rest, one finds again that the steady vorticity equation is either elliptic or hyperbolic, and the unsteady vorticity equation is always hyperbolic. Hence it is precisely waves of vorticity which propagate into rest.

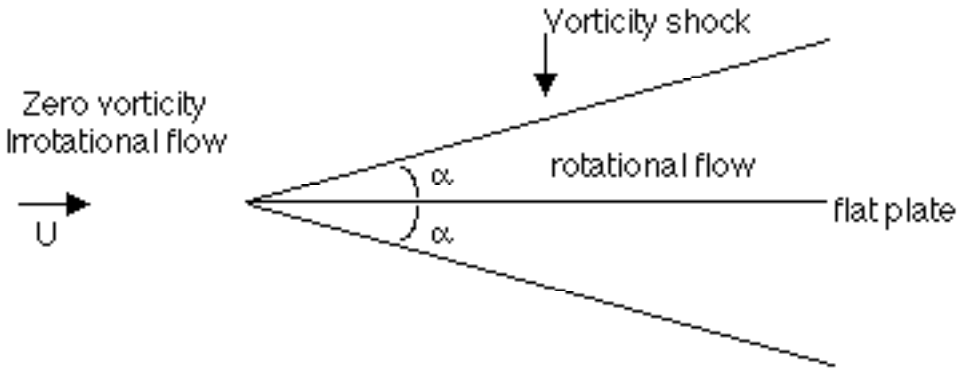

Figure 7 Mach wedge for the vorticity, $\tan \alpha = (1-M^2)^{-1/2}$.

The mathematical consequences of composite roots are clearly evident in the recent solutions of L. E. Fraenkel [1987], H. Hu [1990], which are reviewed in Joseph's [1990] book, of the problem of linearized supercritical flow over a flat plate. The linearization here is around the uniform flow which exists at infinity, as in Oseen's problem for the Navier-Stokes equation.

Fraenkel's solution shows that there is a Mach wedge of vorticity ζ centered on the leading edge of the plate. The vorticity in front of this wedge is zero and it is not zero behind the wedge [see Figure 7]. Surprisingly, the vorticity jumps from zero to infinity at the wedge, but the singularity is integrable. We have rotational flow behind the shock and irrotational flow in front of the shock. The stream function satisfies $^2\Psi=-\zeta$ where $\zeta=0$ in front of the shock. Therefore, we may write $\Psi=\Psi_1+\Psi_2$, $^2\Psi_2=-\zeta$, $^2\Psi_1=0$. To satisfy the boundary conditions on the plate, we must have a nonzero potential field Ψ_1. In fact Ψ_1 satisfies a Dirichlet problem for the region outside a strip on the positive x axis.

The potential flow decays to uniform flow as one moves upstream, but the delay is slow. There is no upstream influence in the fully hyperbolic flow of a gas over a flat plate. The upstream influence of the flat plate in the flow of a Newtonian fluid is almost negligible. The persistence of Ψ_1 is a consequence of its ellipticity, ultimately to the fact that the first order system is of composite type. This type of solution may be new in mathematical physics.

The velocity and the stresses decompose into harmonic and vortical parts. Hence these fields are all of composite type. Only the vorticity is pure, strictly hyperbolic in the linearized problem of flow past bodies. The velocity and stresses are continuous across the shock. The normal derivative of the velocity, the normal and shear stress are also continuous, but the tangential derivative of the tangential components of velocity and stress are discontinuous. The elliptic component of our composite system is associated with a huge upstream influence.

Similar considerations enter into the dynamics of flow over small cylinders which we discussed in §1 of this paper. Delvaux and Crochet [1990] gave a numerical solution of the problem of flow over a cylinder using the constitutive equation of an upper convected Maxwell model. This solution is reviewed in the book of Joseph [1990]. Their solution is fully nonlinear and it supports the notion that the anomalous heat transport and drag observed in the experiments are associated with a change of type. A different numerical solution based on the algorithm

SIMPLER has been given by Hu and Joseph [1990] and it agrees with the numerical solution of Delvaux and Crochet. Aspects of the solution of Hu and Joseph are discussed below.

In the present problem we wish to evaluate the effect of viscoelasticity upon the heat transfer and drag. An upper convected Maxwell model is used. We assume that the viscous heating is negligible and that temperature differences in the flow are small and such that the fluid properties (ρ, λ and η) do not change. Then the temperature field is decoupled from the velocity field, the energy equation is simply

$$c_p \rho (\mathbf{u} \cdot) T = \kappa \Delta T \tag{11}$$

where T is the temperature, c_p the heat capacity and κ the thermal conductivity.

We shall scale length with the diameter of the cylinder d, velocity with the free stream velocity U, pressure with ρU^2 and stress with $\eta U/d$, and use the same symbol for the dimensional and dimensionless quantities. In the dimensionless form the equations of the momentum, the constitutive equation and the temperature are

$$(\mathbf{u} \cdot) \mathbf{u} = - \nabla p + \frac{1}{\leftarrow} \Delta \mathbf{u} + \frac{1}{\leftarrow} \nabla \cdot \boldsymbol{\tau}_E , \tag{12}$$

$$W\left[(\mathbf{u} \cdot \nabla) (\boldsymbol{\tau}_E + \boldsymbol{\tau}_N) - \nabla \mathbf{u} (\boldsymbol{\tau}_E + \boldsymbol{\tau}_N) - (\boldsymbol{\tau}_E + \boldsymbol{\tau}_N) \nabla \mathbf{u}^T \right] + \boldsymbol{\tau}_E = 0, \tag{13}$$

$$\leftarrow \mathrm{Pr} (\mathbf{u} \cdot) T = \Delta T \tag{14}$$

where for the convenience of numerical treatment the extra stress is split into two parts $\boldsymbol{\tau} = \boldsymbol{\tau}_N + \boldsymbol{\tau}_E$ with $\boldsymbol{\tau}_N = 2\eta \mathbf{D}$ being the pseudo-Newtonian part and $\boldsymbol{\tau}_E$ being the part due to the elasticity. The dimensionless temperature is taken as $(T-T_\infty)/T_\infty$ (T_∞ is the temperature of the coming fluid). In these equations the non-dimensional parameters $\leftarrow$ (Reynolds number), W (Weissenberg number), Pr (Prandtl number) are defined as

$$\leftarrow = \rho U d/\eta \ ,$$

$$W = \lambda U/d \ ,$$

$$Pr = c_p \rho/\kappa \ . \tag{15}$$

It is helpful to introduce another two non-dimensional parameters, the viscoelastic Mach number M and the elasticity number E which are defined by

$$M = \sqrt{W\leftarrow} = \leftarrow\sqrt{E} = \frac{U}{c} \ ,$$

$$E = \frac{W}{\leftarrow} = \frac{\eta\lambda}{\rho d^2} \ , \tag{16}$$

where

$$c = \sqrt{\frac{\eta}{\lambda\rho}} \tag{17}$$

is the speed of shear waves in a Maxwell fluid. In the study of change of type the Mach number M is an essential parameter. The elasticity number E depends only on the fluid properties and the flow geometry. In our computation we choose the pair (←,E) as the independent parameters, and simulate the flow in experiments by keeping E fixed and adjusting ←.

In the computation we solve for the velocities, the pressure and the stresses in each iteration. Since the temperature field does not effect the velocity, the heat equation is solved after the iteration converges. Some additional quantities are also calculated. We evaluate the stream function ψ and the vorticity ω which are defined by

$$u_r = -\frac{\partial\psi}{r\partial\theta} \ , \ u_\theta = \frac{\partial\psi}{\partial r} \ , \tag{18}$$

$$\omega = \frac{\partial u_\theta}{\partial r} + \frac{u_\theta}{r} - \frac{\partial u_r}{r\partial\theta} \ . \tag{19}$$

From the computed values of the pressure and the pseudo-Newtonian stresses on the surface of the cylinder it is easy to obtain the drag force acting on the cylinder. The dimensional drag force per unit length on the cylinder is found to be

$$F_x = \rho U^2 d \int_0^{\pi} [\, p \cos\theta + \frac{1}{\leftarrow} \tau_{Nr\theta} \sin\theta]_{r=d/2} \, d\theta \,, \tag{20}$$

which has two contributions, one from the pressure and the other from the pseudo-Newtonian shear stress. In writing (20) we noted that the contribution to the drag of the elastic part of the extra stress vanishes because $\tau_{Er\theta}=0$ on the surface of the cylinder. The drag coefficient is given by

$$C_D = \frac{F_x}{\frac{\rho}{2} U^2 d} \tag{21}$$

In our computation of heat transfer, we prescribe the upstream temperature as T_∞ (in dimensionless form T=0), and the temperature on the cylinder surface as $T_0=2T_\infty$ (in dimensionless form T=1). The dimensional average heat flux from the cylinder to the surrounding fluid is

$$Q = \frac{1}{\pi} \int_0^{\pi} \left[\kappa \frac{\partial T}{\partial r} \right]_{r=d/2} d\theta \,. \tag{22}$$

Thus the Nusselt number which characterizes the heat transfer from the cylinder to the surrounding fluid is defined as

$$Nu = \frac{Qd}{\kappa(T_0 - T_\infty)} = \frac{Qd}{\kappa T_\infty} \,. \tag{23}$$

We next keep the flow fixed at a certain Reynolds number and vary the elasticity number, thus we can look at the effect of the elasticity of the fluid on the flow. Figure 8 presents the streamlines in the neighborhood of the cylinder for flows at $\leftarrow$=10 and E varying from 0 to 1.0. (a) and (b) are almost identical. Starting from (c) with M greater than one, we see an increasingly

larger downstream shift of the streamlines, at the same time there is a relatively small upstream shift. The streamline pattern with viscoelastic fluids of large elasticity number differs significantly from that with Newtonian fluids. The large distortion of the streamlines creates a wide region near the cylinder where the velocity is very low, thus affects the total drag on the cylinder and the heat transfer from the cylinder to the surrounding fluid as we will see later.

Figure 8 Streamlines in the neighborhood of the cylinder for the flow of the same Reynolds number $\leftarrow$=10 and different elasticity number E. (a) E=0 (M=0). (b) E=0.01 (M=1.0). (c) E=0.1 (M=3.16). (d) E=0.25 (M=5.0). (e) E=0.5 (M=7.07). (f) E=1.0 (M=10). In the figures the values of the incoming streamlines, starting from the bottom, are 0.01, 0.05, 0.2, 0.4, 0.6, 0.8, 1.0, 1.2, 1.4, 1.6, 1.8, 2.0, 2.2 and 2.4 respectively.

Figure 8 shows the isovorticity lines at $\leftarrow$=10 and E varying from 0 to 1.0. (a) is the familiar Newtonian case, where the isovorticity lines are swept downstream by the flow and the high vorticity region is at the front shoulder of the cylinder surface where the vorticity is being created. (b) is basically the same as (a) except at the front of the cylinder where the isovorticity lines are closer together signaling a sharper change of vorticity in this region. In (c), at a Mach number M=3.16, we see that the isovorticity lines jam together at the front of the cylinder thus creating a vorticity shock, like a blunt body shock in gas dynamics. As the elasticity number increases, this shock still exists and moves slightly upstream. In Figure 8(d) to 8(f), the picture of the isovorticity lines for viscoelastic fluids with large relaxation time is drastically different from that of Newtonian fluids. Besides the high vorticity zone on the front shoulder of the cylinder surface which occurs already in the Newtonian case, there exists a second high vorticity region which starts to build up and shifts away from the cylinder surface as the elasticity number increases. We find that the maximum values of the vorticity in this second region are even higher than the maximum values of the vorticity on the cylinder surface, which suggests generation of the vorticity away from the cylinder surface or behind the shock. We still do not understand the physical consequences of this build up. The existence of this second high vorticity region away

from the cylinder surface was also observed in the work of Delvaux and Crochet [1990]; they found a local minimum and maximum in the vorticity plot along a path just above the cylinder ($\theta=\pi/2$). The dashed lines in Figure 9 indicate the angles, $\beta=\tan^{-1}\frac{1}{\sqrt{1-M^2}}$, of vorticity shocks predicted in the linear theory in which the governing equations are linearized around the uniform income flow. Close to the cylinder, the vorticity shock is strong. The nonlinearity makes the shock curve around the cylinder. As E increases, the nonlinear region also increases due to the large stagnant region around the cylinder. Since the linear theory is valid far away from the cylinder, the vorticity shock, if it exists, should eventually stretch with the angle predicted in the linear theory. But because the the shock is weak and the numerical space discretization is usually coarse far away from the cylinder, it is very hard to capture this part of the shock numerically.

Figure 9 Isovorticity lines for the flow of the same Reynolds number $\leftarrow=10$ and different elasticity number E. (a) E=0 (M=0). (b) E=0.01 (M=1.0). (c) E=0.1 (M=3.16). (d) E=0.25 (M=5.0). (e) E=0.5 (M=7.07). (f) E=1.0 (M=10). The dashed lines in the figures indicate the angle of the vorticity shocks predicted in the linearized theory.

The velocity component u in the direction of the free stream is presented in Figure 10 for $\leftarrow=10$ and E=0, 0.01, 0.1, 0.25, 0.5, 1.0. Figure 10(a) gives the profile of u ahead of the cylinder along the ray $\theta=0$. 10(b) gives the profile just above the cylinder along the ray $\theta=\pi/2$. It is clear that for the flows of larger E, there is a region with small velocity close to the cylinder. This stagnant region grows with E. The diameter of this region has increased to about 3 times the cylinder diameter when E=1 as seen in Figure 10(b). Figure 10(a) also shows that there is a strong upstream influence for the viscoelastic flow with large E. In 10(b) we notice a velocity over-shoot in the region above the cylinder. This over-shoot exists for all cases with $M>1$ and shifts away from the cylinder as E increases. The slope of the velocity profile in (b) is consistent with the vorticity (derivatives of the velocity) distribution above the cylinder, and indicates a second high vorticity region away from the cylinder surface.

Numerical integration is carried out for (20) on the cylinder surface to get the drag force acting on the cylinder. The drag coefficient C_D is plotted in Figure 11 as a function of ← for four values of E= 0, 0.01, 0.1 and 1. The results for E=0, 0.01 and 0.1 are obtained using mesh No.2. For E=1 the results using the other two meshes are also presented. We see that the mesh refinement has little influence on the drag coefficient for the range of parameters in our computation. In the figure we indicated the critical values of ← at which M=1 for different E's (for E=1, ←=1; E=0.1, ←=3.16 and E=0.01, ←=0.1). As ← increases beyond these critical values, the drag coefficient curves for viscoelastic flows begin to separate from the curve for Newtonian flow. The deviation is more evident for flows with large E. In the region of supercritical flow, M>1, we see that the effect of the viscoelasticity is to increase the drag. This is consistent with the observation in the streamline plot Figure 8, which shows a nearly stagnant region around the cylinder. This stagnant region effectively increases the size of the cylinder, thus increases the total drag.

Figure 10 Effects of viscoelasticity on the velocity profile. The results are obtained with ←=10 and E = 0, 0.01, 0.1, 0.25, 0.5, 1. u is the velocity component in the direction of the free stream. (a) u versus r along the path θ=0, ahead of the cylinder. (b) u versus r along the path θ=π/2, just above the cylinder.

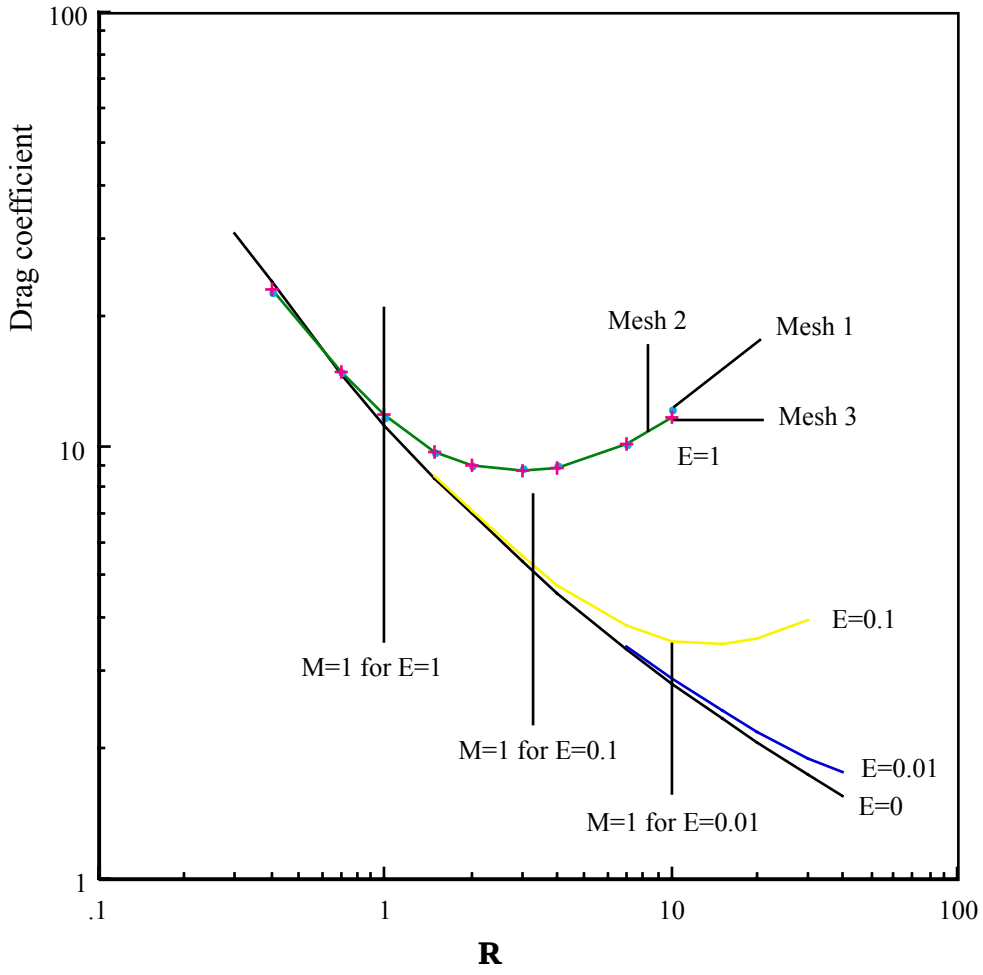

Figure 11 Drag coefficient C_D versus Reynolds number ← for elasticity number E=0 (Newtonian), 0.01, 0.1 and 1.0. Results for solid lines are obtained using mesh No.2. For E=1, the results obtained by the other two meshes are also plotted. The dashed lines indicate the values of Reynolds number at which the viscoelastic Mach number M=1.

The formula for the drag force acting on the cylinder (20) shows that the total drag can be separated into two parts, one part due to the pressure distribution around the cylinder and the other part due to the shear stress on the cylinder surface. These two contributions of the drag are plotted in Figure 12. In the figure, the drag coefficients of a viscoelastic case E=0.1 is compared

with those of the Newtonian case E=0. In the Newtonian case, when ← is small, the drag coefficients due to pressure and due to shear stress are equal, as is well known. The pressure drag coefficient increases with ← because of the wake generated behind the cylinder. This is especially true in the viscoelastic case, where the drag due to pressure can be much larger than the drag due to shear stress, as we see in the figure, since we have larger wakes in viscoelastic cases. The nearly stagnant region around the cylinder is also responsible for the reduction of the drag due to the shear stress in viscoelastic flow.

Figure 13 presents graphs of the Nusselt number Nu versus ← for E=0, 0.01, 0.1 and 1 at Pr=1 and Pr=10. We checked the results for E=1 with three meshes. The results are almost identical. Again the values of ← at which M=1 are indicated in the figure with dashed lines. For ← less than these critical values, the Nusselt number for viscoelastic flow is the same as that for Newtonian flow. For ← greater than the critical values, the Nusselt number deviates from the Newtonian path and tends to an asymptotic value which does not depend on ←. This deviation is more prominent for large E and Pr. We see that the effect of the viscoelasticity is to decrease the Nusselt number, or to reduce the heat transfer from the cylinder to the surrounding fluid. This can also be explained by the stagnant region which develops around the cylinder when the flow becomes supercritical (M>1).

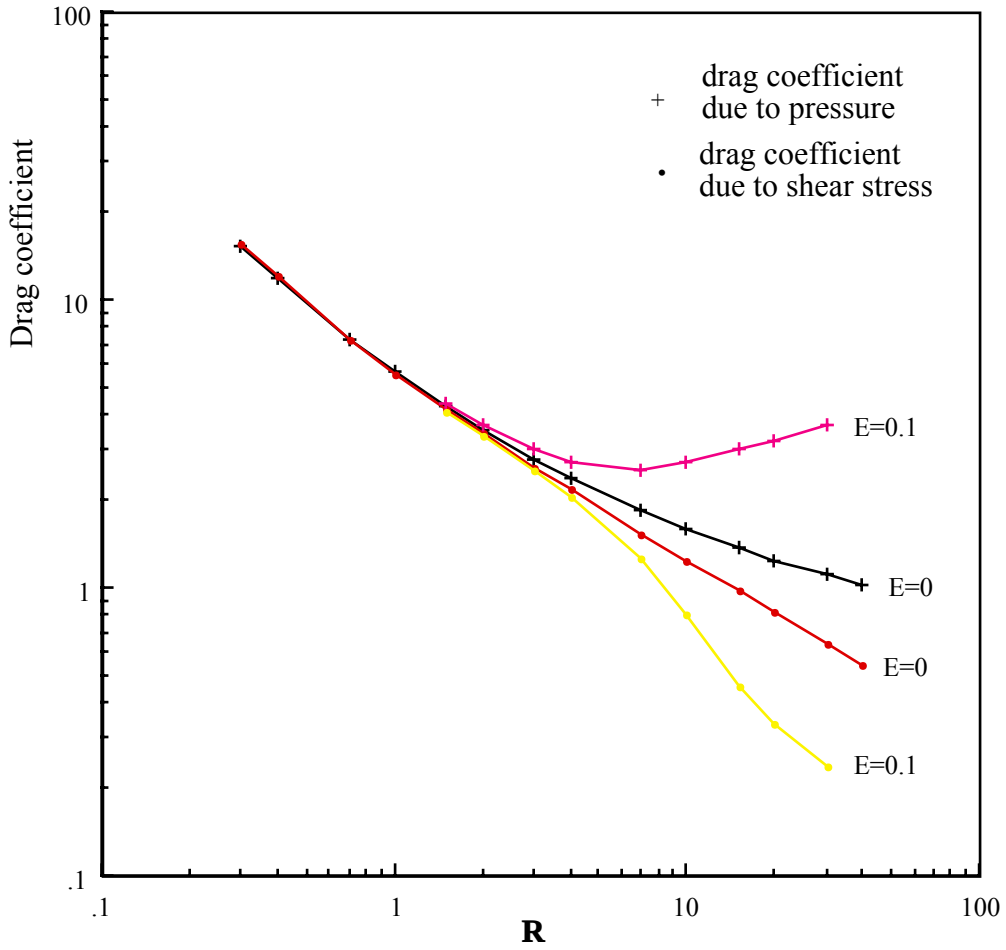

Figure 12 Effect of the elasticity of the fluids on the drag due to pressure and the drag due to shear stress on the cylinder surface.

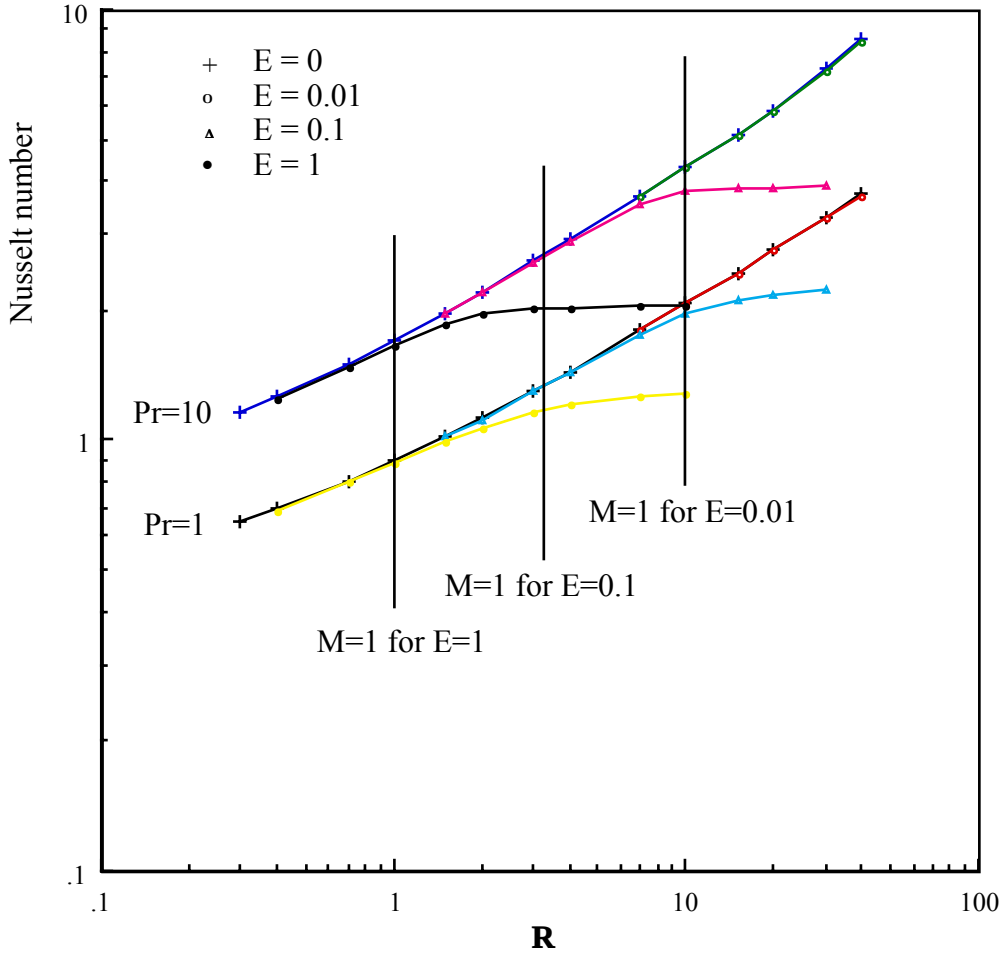

Figure 13 Nusselt number Nu versus Reynolds number ← for different elasticity numbers E=0 (Newtonian), 0.01, 0.1, 1.0, and at Prandtl number Pr=1 and 10. The dashed lines indicate the values of Reynolds number at which the viscoelastic Mach number M=1.

For the drag coefficient, the experiments of James and Acosta [6] were carried out on a wire of diameter 0.005in. in solutions of Polyox WSR-301. The intrinsic viscosity of WSR-301 was $[\eta]$=9.6 g/100ml measured in the experiments. We reproduced the data for concentration ϕ=15.7, 30, 60, 119 and 226 ppmw in Figure 14. The shear wave speed for WSR-301 of

concentration 50 ppm is about 2.48 cm/s, which is measured using a wave speed meter and listed in the tables of Joseph [1990]. Using this wave speed, we can get the shear wave speeds for the other concentrations from relation (5). Thus we estimate that elasticity numbers E=0.03 for the set of data of 15.7 ppm, E=0.07 for 30 ppmw, E=0.13 for 60 ppm, E=0.3 for 119 ppm and E=0.6 for 226 ppm as indicated in Figure 14. These values are much larger, about 50 times larger, than the values estimated in James and Gupta [1971]. As shown in Figure 14, the agreement is fair.

In the Nusselt number Figure 1 we have reproduced the experimental data for distilled water and for Polyox WSR-301 of concentrations 26.2, 52.4, 119 and 226 ppmw with three wire diameters, d=0.006in., 0.002in. and 0.001in. The elasticity numbers are similarly estimated and indicated in the figures. The experimental value of Pr is not known exactly, for distilled water at 20°C the Prandtl number is about 7. Thus the numerical results plotted in lines are obtained with Pr=7. Qualitatively, the numerical results show the same tendency of the experimental results. The differences, we think, are due to many factors. Our estimation of the elasticity number is rough, as we see from (33), a 10% error in the shear wave speed causes 20% difference in E. The heat transfer experiments were carried out with a temperature difference varying from 9-33°C. This temperature difference changes the viscosity and the shear wave speed of the solution, thus causes differences in the E. Also our choice of Maxwell model with a single relaxation time to characterize the fluid is certainly not optimal.

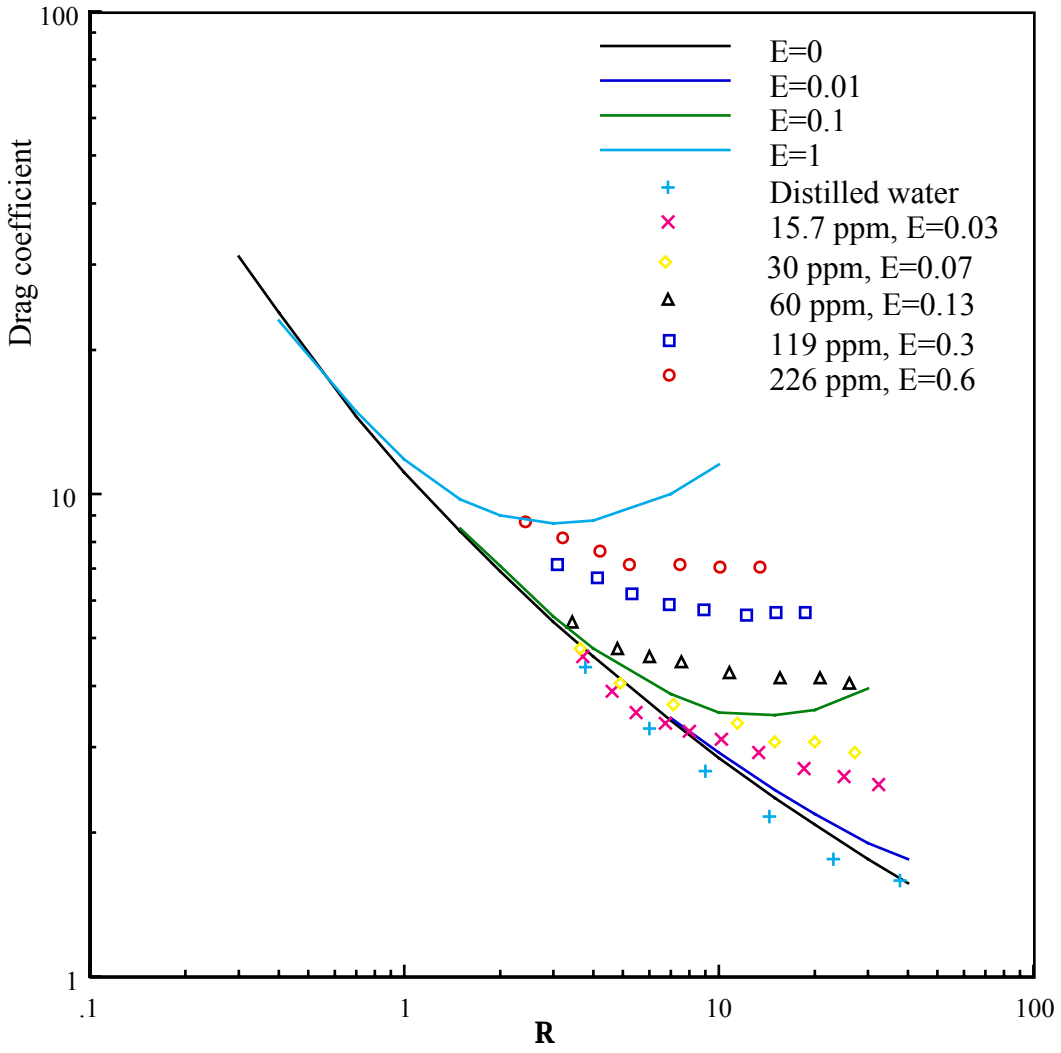

Figure 14 Comparison of the drag coefficient obtained by present computation (lines) with those measured in experiments of James and Acosta [6] (dots). The elasticity numbers for the experimental data are estimated using the shear wave speed as described.

ACKNOWLEDGEMENT

This work was supported by the Army Research Office, National Science Foundation and Department of Energy.

REFERENCES

Ahrens, M., Yoo, J. Y. and Joseph, D. D. Hyperbolicity and change of type in the flow of viscoelastic fluids through pipes, *J. Non-Newtonian Fluid Mech.,* Vol. **24**, pp. 67–83, 1987.

Ambari, A., Deslouis, C. and Tribollet, B. Coil-stretch transition of macromolecules in laminar flow around a small cylinder, *Chem. Eng. Commun.,* Vol. **29**, pp. 63–78, 1984.

Coleman, B. and Noll, W. An approximation theorem for functionals with applications in continuum mechanics, *Arch. Rat. Mech. Anal.,* Vol. **6**, pp. 355–370, 1960.

DELVAUX, V. AND CROCHET, M.J. 1990 Numerical simulation of delayed die swell. *Rheologica Acta* **29**, to appear.

DELVAUX, V. AND CROCHET, M.J. 1990 Inertial viscoelastic flow past circular cylinder. *J. non-Newtonian Fluid Mech.,* to appear.

Fraenkel, L. E. Some results for a linear, partly hyperbolic model of viscoelastic flow past a plate, in *Material Instabilities in Continuum Mechanics and Related Mathematical Problems* (ed. J. M. Ball), Clarendon Press, Oxford, 1987.

James, D. and Acosta, A. J. The laminar flow of dilute polymer solutions around circular cylinders, *J. Fluid Mech.,* Vol. **42**, pp. 269–288, 1970.

James, D.F. and Gupta, O.P. Drag on circular cylinders in dilute polymer solutions, *Chem. Eng. Progr.* **67** Nº 111, 62–73, 1971.

Joseph, D.D. *Fluid Dynamics of Viscoelastic Liquids.* Springer, 1990.

Joseph, D. D., Matta, J. and Chen, K. Delayed die swell, *J. Non-Newtonian Fluid Mech.,* Vol. **24**, pp. 31–65, 1987.

Joseph, D.D. and Saut, J.C. Change of type and loss of evolution in the flow of viscoelastic fluids, *J. non-Newtonian Fluid Mech.* **20**, 117–141, 1986.

Konuita, A., Adler, P. M. and Piau, J. M. Flow of dilute solutions around circular cylinders, *J. Non-Newtonian Fluid Mech.,* Vol. **7**, pp. 101–106, 1980.

Metzner, A.B., Uebler, E.A., and Fong, C.F.C.M. Converging flows of viscoelastic materials, *AIChE J.* **15**, 750–758, 1969.

Renardy, M., Hrusa, W. J. and Nohel, J. A. *Mathematical Problems in Viscoelasticity,* Longman, Harlow, UK, 1987.

Rutkevich, M. I. Some general properties of the equations of viscoelastic fluid dynamics, *PMM,* Vol. **33**, pp. 42–51, 1969.

Saut, J. C. and Joseph, D. D. Fading memory, *Arch. Rat. Mech. Anal.,* Vol. **81**, pp. 53–95, 1983.

Slemrod, M. Breakdown of smooth shearing flow in viscoelastic fluids for two constitutive equations; the vortex sheet vs. the vortex shock. Appendix to the paper by Joseph, D. D. Hyperbolic phenomena in the flow of viscoelastic fluids, in *Viscoelasticity and Rheology* (eds. A. S. Lodge, J. Nohel and M. Renardy), Academic Press, 1985.

Ultman, J. S. and Denn, M. M. Anomalous heat transfer and a wave phenomenon in dilute polymer solutions, *Trans. Soc. Rheol.,* Vol. **14**, pp. 307–317, 1970.

Yoo, J.Y., Ahrens, M., and Joseph, D.D. Hyperbolicity and change of type in sink flow, *J. Fluid Mech.* **153**, 203–214, 1985.

Yoo, J. and Joseph, D. D. Hyperbolicity and change of type in the flow of viscoelastic fluids through channels, *J. Non-Newtonian Fluid Mech.,* Vol. **19**, pp. 15–41, 1985.